



Experimental, Theoretical and Monte Carlo simulation of quinoline derivative as effective corrosion inhibitor for mild steel in 1 M HCl

H. Lgaz^{1,2}, R. Salghi^{2*}, M. Larouj¹, M. Elfaydy³, S. Jodeh⁴,
Z. Rouifi^{1,3}, B. Lakhrissi³, H. Oudda¹

¹Laboratory separation processes, Faculty of Science, University Ibn Tofail PO Box 242, Kenitra, Morocco.

²Laboratory of Environmental Engineering and Biotechnology, ENSA, Ibn Zohr University, PO Box 1136, 80000 Agadir, Morocco

³Laboratoire d'Agroressources, Polymères et Génie des Procédés, University Ibn Tofail PO Box 242, Kenitra, Morocco.

⁴Department of Chemistry, An-Najah National University, P. O. Box 7, Nablus, Palestine

Received 16 Aug 2016, Revised 30 Sept 2016, Accepted 5 Oct 2016

*For correspondence: Emails: r.salghi@uiz.ac.ma (R. Salghi); Phone: +212 6 61145512

Abstract

The corrosion behaviour of 5,5'-(((2-hydroxypropane-1,3-diyl)-bis-(oxy))-bis-(methylene))-bis-(8-quinolinol) noted **HBQ8** towards mild steel has been studied for corrosion inhibition of mild steel in 1 M hydrochloric acid (HCl) by weight loss, Tafel polarization and electrochemical impedance spectroscopy (EIS) techniques. Then the experimental results were confirmed by molecular dynamic simulation and DFT calculations. The results showed that the inhibition efficiency (% IE) of **HBQ8** increased with increasing inhibitor concentration and decreased with increase in temperatures. It was found that **HBQ8** behaved as a mixed type inhibitor. The adsorption process of inhibitor obeyed the Langmuir isotherm and the thermodynamic parameters were discussed. The results from the weight loss, electrochemical measurements and theoretical calculations are in good agreement.

Keywords: Corrosion inhibition, quinoline, DFT, Monte Carlo simulation, mild steel

1. Introduction

Mild steel is known to be a very versatile ferrous alloy utilized for a wide range of applications [1-8]. It is extensively used in various industries as construction material for chemical reactors, heat exchanger and boiler systems, storage tanks and oil and gas transport pipelines [9, 10]. Acid solutions are widely used in industry for processes such as acid pickling, chemical cleaning and oil well acidification. The higher solubility of hydrochloric acid in aqueous medium causes the least polarizing effect and does not hinder the rate of corrosion [11-18].

A continuing effort has been made to develop a corrosion inhibitor that exhibits a greater inhibition effect at a low concentration in the corrosion medium as well as environment-friendly feature [19]. Most of the acid corrosion inhibitors are organic compounds containing electronegative atoms (such as O, N, S and P *etc.*), unsaturated bonds and/or aromatic rings. The inhibitory performance of organic compounds is due to the adsorptive layer forming between the molecules with lone electron pair and/or π electrons and the surface metal atoms with unoccupied d-orbitals [20, 21]. Meanwhile, the use of quantum chemical calculations has been proved to be a useful tool in elucidating the mechanism of inhibition of corrosion inhibitors on metal surface at the molecular level; and, it can provide theoretical support in searching for new inhibitors [22, 23].

The compounds with quinolone functions are rarely investigated such as corrosion inhibitors [24, 25]. Therefore, it is necessary to study the corrosion inhibition effect and inhibition mechanism of the quinoline derivatives which could be deemed as good potential inhibitors.

In this paper, we employed electrochemical techniques, weight loss method to study the inhibition effect of new quinoline derivatives namely, 5,5'-(((2-hydroxypropane-1,3-diyl)-bis-(oxy))-bis-(methylene))-bis-(8-quinolinol) (**HBQ8**) for mild steel in 1.0 M HCl solution. And then, quantum chemical calculations by Molecular dynamic simulation and DFT method were performed to elucidate the interaction between the inhibitor molecules and mild steel surface.

2. Materials and methods

2.1. Synthesis

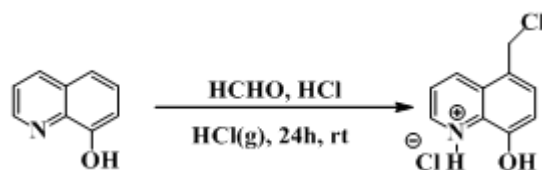
❖ General Information

All chemicals products were obtained from commercial suppliers Aldrich or Acros (France or Spain), and were used without further purification. NMR spectra were recorded on a model Bruker Avance (300 MHz) for solutions in Me₂SO-d₆, and Chemical shifts are given as δ values with reference to tetramethylsilane (TMS) as internal standard. The progress of the reaction was followed by Thin-Layer Chromatography (TLC) using silica gel 60 F254 (E. Merck) plates with visualization by UV light (254 nm). The melting points were determined on an automatic electrothermal IA 9200 digital.

❖ Chemical synthesis

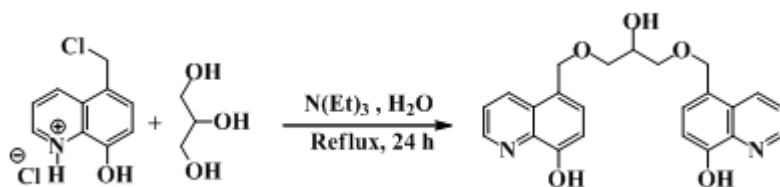
Synthesis of 5,5'-(((2-hydroxypropane-1,3-diyl)-bis-(oxy))-bis-(methylene))-bis-(8-quinolinol)

The preparation of 5,5'-(((2-hydroxypropane-1,3-diyl)-bis-(oxy))-bis-(methylene))-bis-(8-quinolinol) (scheme 1) require at first, the preparation of 5-(chloromethyl)-8-hydroxy-quinoline hydrochloride, which was obtained according to the method described by Fernando et al. [26].



Scheme 1: Synthesis of 5-chloromethyl-8-quinoline hydrochloride

The condensation of 5-chloromethyl-8-quinolinol hydrochloride (CMQ) with glycerol in the presence of triethylamine gives the corresponding 5-disubstituted product (Scheme 2).



Scheme 2: Synthesis of 5,5'-(((2-hydroxypropane-1,3-diyl)-bis-(oxy))-bis-(methylene))-bis-(8-quinolinol).

5-Chloromethyl-8-hydroxyquinoline hydrochloride (4.99 g, 0.0217 mol) in 20 ml of bi-distilled water were added over 30 min into a solution of the glycerol (1 mL, 0.0109 mol), 10 mL of bi-distilled water, and (3 mL, 0.0217 mol) of triethylamine. The mixture was stirred under 95 °C for 24 h, after completion of the reaction (monitored by TLC using a mobile phase consisting of acetone-n-hexane-e (30:70, v/v). The resulting precipitate was filtered, washed thoroughly with bi-distilled water, dried and crystallized from ethanol to afford 1.74 g. of pale yellow solid in 40 % yield, m.p.: 140-142 °C, R_f value: 0.81 (n-hexane-acetone: 70:30, v/v).

^1H NMR (300 MHz, DMSO- d_6), $\delta_{\text{ppm}} = 8.85\text{-}8.84$ (s, 2 H, quinoline (OH)), 6.99-8.84 (m, 10 H, quinoline (C-H)), 4.72 (s, 4H, quinoline -CH₂-O), 3.50 (s, 1H, OH of glycerol), 3.23-3.25 (d, 4 H, O-CH₂-C), 3.81-3.84 (m, 1 H, -CH-O).

^{13}C NMR (300 MHz, DMSO- d_6), $\delta_{\text{ppm}} = 63.59$ (-CH₂-CH-OH of glycerol), 70.78 (quinoline-CH₂-O), 72.21 (O-CH₂-CH), 111.06 -152.42 (CH-C quinoline).

^1H NMR spectra (300 MHz, DMSO- d_6)

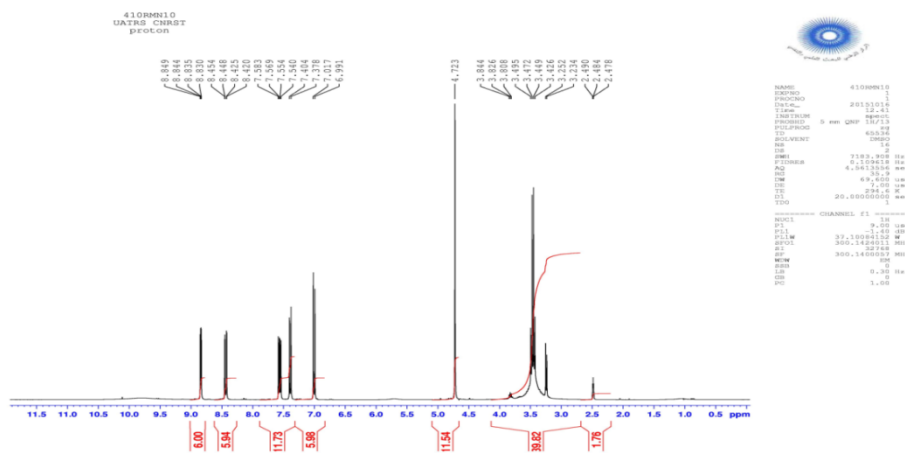


Figure 1: ^1H NMR spectrum of 5,5'-(((2-hydroxypropane-1,3-diyl)-bis-(oxy))-bis-(methylene))-bis-(8-quinolinol)

^{13}C NMR spectra (300 MHz, DMSO- d_6)

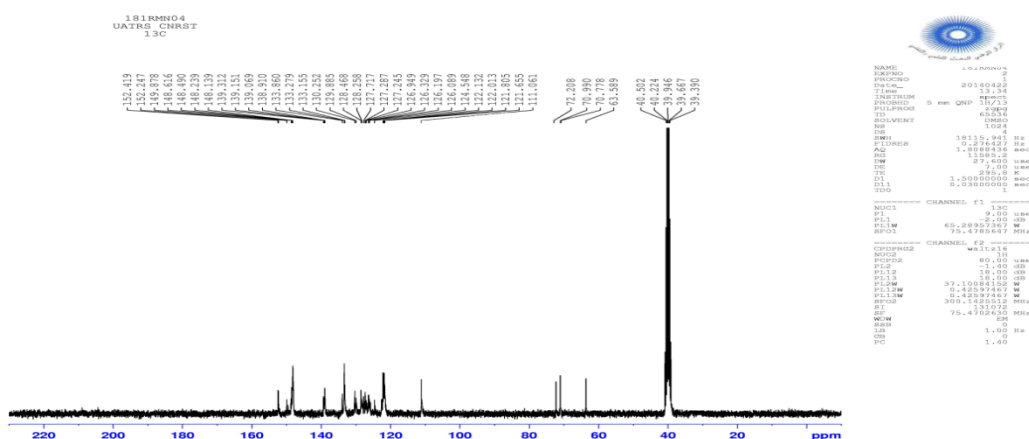


Figure 2: ^{13}C NMR spectrum of 5,5'-(((2-hydroxypropane-1,3-diyl)-bis-(oxy))-bis-(methylene))-bis-(8-quinolinol)

2.2. Gravimetric, Electrochemical measurements and Electrolytic solution

The gravimetric measurements were carried out at definite time interval of 6 h using an analytical balance (precision ± 0.1 mg), The steel specimens of dimension $2 \times 2 \times 0.08$ cm³ used in this study is a carbon steel: (Euronorm: C35E carbon steel and US specification: SAE 1035) with a chemical composition (in wt%) of

0.370% C, 0.230% Si, 0.680% Mn, 0.016% S, 0.077% Cr, 0.011% Ti, 0.059% Ni, 0.009% Co, 0.160% Cu and the remainder iron (Fe). The surface of the test electrode was mechanically abraded by different grades of emery papers with 220 up to 1500, washed with distilled water, cleaned with acetone after being weighed accurately with high sensitivity balance, the specimens were carried out in a double glass cell equipped with a thermostated cooling condenser containing 80 mL of non-de-aerated test solution with and without various concentrations of the studied quinoline derivatives (**HBQ8**) at 303K, and at different temperatures (303 – 333K) for 10^{-3} M concentration. After immersion period, the specimens were taken out, rinsed thoroughly with bidistilled water, dried and weighed accurately again. Five tests were performed in each case and the mean value of the weight loss was calculated. The electrochemical experience have been performed using an equipment of impedance (Tacussel Radiometer PGZ 100), the data were analyzed using software VoltaMaster 4. A cell of Pyrex glass with three cylindrical electrodes has been used. To control temperature a thermostat has been used. A platinum auxiliary electrode and saturated calomel electrode (SCE) as reference electrode. The working electrode was carbon steel with the surface area of 1 cm^2 . All potentials are reported vs. SCE. Prior to the electrochemical experiments, the mild steel was immersed into the test solution for 30min until a steady-state (open circuit) potential was obtained. EIS measurements were performed with a frequency range of 10 mHz to 100 kHz and amplitude of 5 mV with 10 points per decade. The polarization curves were recorded by polarization from -800 to -200 mV/SCE with a scan rate of 60 mV s^{-1} . ZView software version 2.8 was used to fit impedance data. Acid solutions (1.0 M HCl) were prepared by diluting a reagent of analytical grade HCl 37% with double-distilled water. The concentration range of the quinoline derivative was used was 10^{-6} to 10^{-3} M.

2.4. Quantum chemical calculations

The quantum chemical calculations were carried out to elucidate the correlation between the inhibitor molecular structure and its efficiency. Quantum chemical calculations were performed using density functional theory (DFT) with the Beck's three parameter exchange functional along with the Lee-Yang-Parr non local correlation functional (B3LYP) with 6-31G (d, p) basis set implemented in Gaussian 03 program package [27-32]. This approach is widely utilized in the analysis of the characteristics of corrosion process. The following quantum chemical parameters were evaluated from the optimized molecular structure: the dipole moment (μ), the energy of the highest occupied molecular orbital (E_{HOMO}), the energy of the lowest unoccupied molecular orbital (E_{LUMO}), the energy band gap ($\Delta E_{\text{gap}} = E_{\text{HOMO}} - E_{\text{LUMO}}$), the electron affinity (A), the ionization potential (I) and the number of transferred electrons (ΔN).

2.5. Molecular dynamic simulation

The Monte Carlo (MC) search was adopted to compute the low configuration adsorption energy of the interactions of the **HBQ8** on a clean iron surface. The Monte Carlo (MC) simulation was carried out using Materials Studio 6.0 software (Accelrys, Inc.) [33]. The Fe crystal was cleaved along the (110) plane, it is the most stable surface as reported in the literature. Then, the Fe (110) plane was enlarged to (12×12) supercell to provide a large surface for the interaction of the inhibitor. The simulation of the interaction between **HBQ8** and the Fe (110) surface was carried out in a simulation box ($29.78 \times 29.78 \times 60.13 \text{ \AA}$) with periodic boundary conditions, which modeled a representative part of the interface devoid of any arbitrary boundary effects. After that, a vacuum slab with 50 \AA thickness was built above the Fe (110) plane. All simulations were implemented with the COMPASS force field to optimize the structures of all components of the system of interest. More simulation details on the methodology of Monte Carlo simulations can be found in previous publications [34, 35].

3. Results and discussion

3.1. Weight loss measurements

3.1.1 Effect of concentration

The values of the inhibition efficiency and corrosion rate (C_R) obtained from weight loss experiments with different concentrations of **HBQ8** in 1.0 M HCl solution at 303 K are presented in Table 1 and Fig. 3. The inhibition efficiency η_w (%) is calculated by the following Eq. 1:

$$\eta_w(\%) = \frac{C_R - C_{R(inh)}}{C_R} \times 100 \tag{1}$$

Where C_R and $C_{R(inh)}$ represent the corrosion rates in the absence and presence of **HBQ8**.

Table 1. Inhibition efficiencies of various concentrations of **HBQ8** for corrosion of mild steel in 1.0 M HCl obtained by weight loss measurement at 303K.

Inhibitor	Concentration (M)	C_R (mg/cm ² ×h)	η_w (%)	Θ
Blank	1.0	1.135	-	-
HBQ8	10 ⁻³	0.087	92.33	0.923
	10 ⁻⁴	0.163	85.64	0.8564
	10 ⁻⁵	0.247	78.24	0.7824
	10 ⁻⁶	0.314	72.33	0.7233

According to [Table 1](#) and [Fig. 3](#), it is observed that the corrosion rates decreases significantly in the presence of the quinoline derivative. The corrosion rates of mild steel in the blank solution was 1.135 mg/cm²×h and the addition of 10⁻³ M of quinoline derivative seed husk reduced the dissolution to 0.087 mg/cm²×h. It should be noted that the inhibition efficiency reaches its maximum value (92.33%) at 10⁻³ M, which indicates that the inhibitor can effectively prevents mild steel from dissolving in the aggressive solution, due to the strong adsorption of quinoline derivative molecule onto the mild steel surface [15-17].

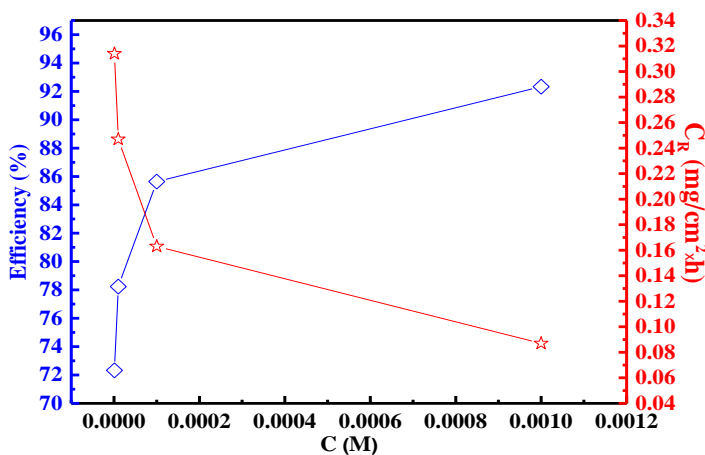


Figure 3: Relationship between the inhibition efficiency, Corrosion rates and inhibitor concentrations for carbon steel after 6 h immersion in 1 M HCl at 303 K.

3.1.2. Effect of temperature

The increase in temperature causes many actions taking place on the solid/liquid interface, such as rapid dissolution of metal substrate and desorption of adsorbed inhibitor molecules [36-37]. In order to evaluate the effect of temperature on the inhibition performance of **HBQ8**, weight loss measurements was performed in 1.0 M HCl in the absence and presence of 10⁻³ M of inhibitor from 303 to 333 K. Results obtained after 6 h exposure time are presented in [Table 2](#), in general, these results reveal that the corrosion rate increased with increase in temperature in both uninhibited and inhibited solutions. Rise in temperature accelerates C_R which results in a

higher dissolution rate of metal [38]. Also the inhibition efficiency is observed to decrease with increase in the temperature. The decrease in inhibition efficiency with temperature might be attributed to desorption of the inhibitor molecules from the metal surface at higher temperatures [39].

To calculate activation parameters of the corrosion process, Arrhenius Eq. (2) and transition state Eq. (3) were used [40]:

$$C_R = k \exp\left(\frac{-E_a}{RT}\right) \quad (2)$$

$$C_R = \frac{RT}{Nh} \exp\left(\frac{\Delta S_a}{R}\right) \exp\left(-\frac{\Delta H_a}{RT}\right) \quad (3)$$

where, E_a is the activation energy, ΔS_a is the entropy of activation, ΔH_a is the enthalpy of activation, k is the Arrhenius pre-exponential factor, h is Planck's constant, N is Avogadro's number, T is the absolute temperature and R is the universal gas constant.

Table 2: C_R and η_w % obtained from weight loss measurements of mild steel in 1.0 M HCl containing 10^{-3} M of **HBQ8** at different temperatures.

Inhibitors	Temperature (K)	C_R ($\text{mg cm}^{-2} \text{h}^{-1}$)	η_w (%)	Θ
Blank	303	1.135	-	-
	313	2.466	-	-
	323	5.032	-	-
	333	10.029	-	-
HBQ8	303	0.087	92.33	0.923
	313	0.368	85.08	0.850
	323	1.234	75.48	0.754
	333	4.011	60.01	0.600

Fig. 4 shows Arrhenius plots of $\ln(CR)$ vs. $1/T$ for mild steel in 1.0 M HCl without and with addition of 10^{-3} M of **HBQ8**. From the value of slope, the value of E_a were calculated for **HBQ8** and listed in Table 3. The results showed that the value of E_a for inhibited solution were higher than those for uninhibited solution. The increase in activation energy could be attributed to an appreciable decrease in the adsorption of the inhibitor on the mild steel surface with increase in temperature [41]. In addition, the increasing E_a may be caused by desorption of inhibitor molecules which takes place on mild steel surface with the increase in temperatures [42, 43].

Using Eq. (3), another linear plot of $\ln C_R/T$ versus $1/T$ was drawn (Fig. 5) with slope $(-\Delta H_a/R)$ and intercept $[\ln(R/Nh) + \Delta S_a/R]$ which was used for the calculation of ΔH_a and ΔS_a . All the values are listed in Table 3. The positive value of ΔH_a reflect that the dissolution process of metal is endothermic [44]. ΔS_a value are more positive in presence of the studied inhibitor compared to free acid solution. The increase of ΔS_a in the presence of inhibitor implies that the activated **HBQ8** in the rate determining step represent an association rather than a dissociation step [45].

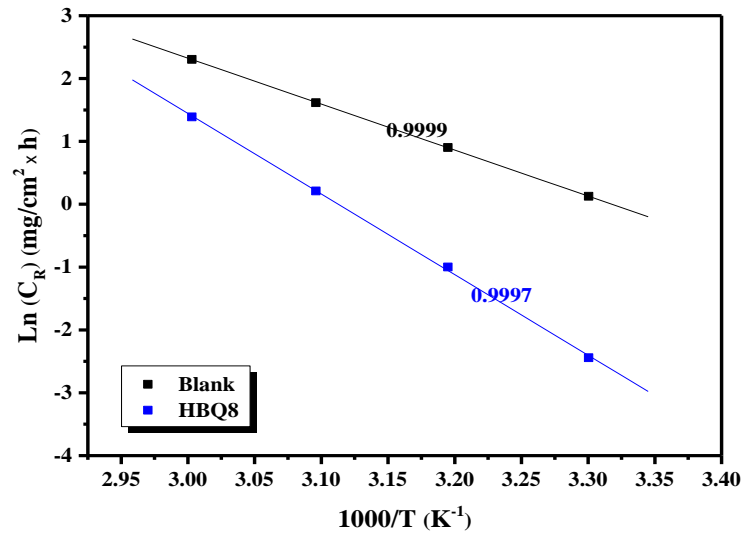


Figure 4: Arrhenius plots for mild steel in 1.0 M HCl in the absence and presence of 10^{-3} M of inhibitor at different temperatures.

Table 3: Activation parameters for mild steel corrosion in 1.0 M HCl in the absence and presence of 10^{-3} M of inhibitor at different temperatures.

Inhibitor	E_a (kJ/mol)	ΔH_a (kJ/mol)	ΔS_a (J/mol \times K)	$E_a - \Delta H_a$
Blank	60.79	58.16	-51.84	2.63
10^{-3} M HBQ8	106.58	103.93	78.21	2.65

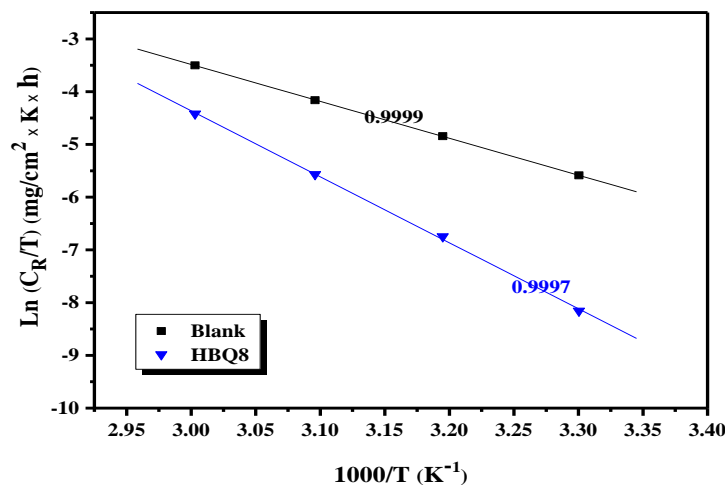


Figure 5: Transition state plots for the inhibition of corrosion of mild steel in 1.0 M HCl in the absence and presence of 1.0 M of inhibitor at different temperatures.

3.2. Adsorption Isotherm

At the metal/solution interface, the adsorption process of organic inhibitor molecules occurs as a result of replacement of H₂O molecules adsorbed on the metallic surface by the following equilibrium (Eq. 4) [46, 47].



where x is the number of H₂O molecules replaced by one organic molecule.

The degree of surface coverage (θ) obtained from potentiodynamic polarisation technique was used to evaluate the best isotherm that fits into the data obtained. Correlation coefficient obtained from the plots of various isotherms such as Langmuir, Freundlich, Temkin were used to determine the isotherms most applicable to experimental data. Langmuir isotherm was applied to investigate whether it best fits to the experimental data obtained by using Eq. (5) [48].

$$\frac{C}{\theta} = \frac{1}{K_{\text{ads}}} + C \quad (5)$$

where C is the inhibitor concentration, θ is the surface coverage and K_{ads} is the adsorption equilibrium constant. The plot of C/θ versus C yields a straight line with a slope close to 1 (1.09) and the linear association coefficient (R^2) is also nearly 1 (0.9999), as shown in Fig. 6, indicating that the adsorption of **HBQ8** on the mild steel surface obeys Langmuir adsorption isotherm. The standard free energy of adsorption (ΔG_{ads}^0) was calculated by using the following expression (Eq. 6) [49].

$$\Delta G_{\text{ads}}^0 = -RT \ln(55.5 \times K_{\text{ads}}) \quad (6)$$

where R is the universal gas constant, 55.5 is the concentration of water in solution and T (K) is the thermodynamic temperature. The calculated values of ΔG_{ads}^0 and K_{ads} for **HBQ8** are listed in Table 4.

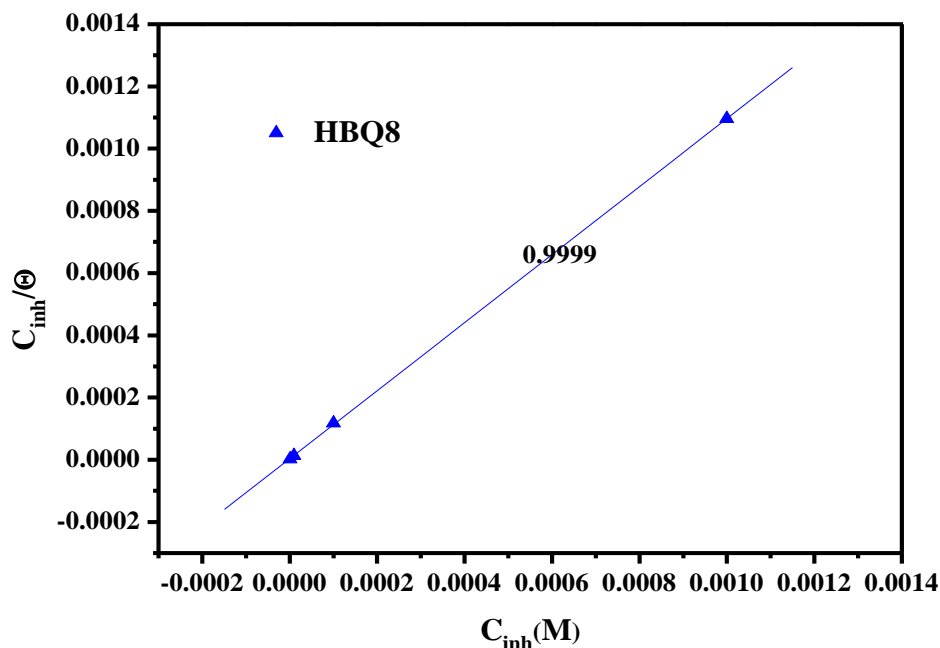


Figure 6: Langmuir adsorption of inhibitor on the carbon steel surface in 1.0 M HCl solution at 303K.

Table 4: Adsorption parameters of inhibitor for mild steel corrosion in 1 M HCl at 303 K.

Inhibitor	Slope	$K_{ads} (M^{-1})$	ΔG_{ads}° (kJ/mol)
HBQ8	1.09	284924.64	-41.74

A high value of K_{ads} indicate that the inhibitor are easily and strongly adsorbed on the metal surface, mean better inhibition efficiency of the inhibitor [50], On the other hand, the high K_{ads} value support the better inhibitive performance of **HBQ8**. The negative value of ΔG_{ads}° ensured the spontaneity of the adsorption process and stability of the adsorbed layer on the mild steel surface [51]. Generally, the values of ΔG_{ads}° around -20 kJ/ mol or more positive are consistent with physisorption, while those around -40 kJ/mol or more negative with chemisorption [52, 53]. The value of ΔG_{ads}° listed in Table 4 may be indicate the predominance of chemisorption of quinoline derivative on the mild steel surface.

3.3. Potentiodynamic Polarization Study

The corrosion of mild steel electrode in 1.0 M HCl solutions containing various concentrations of **HBQ8** was studied by potentiodynamic polarization. Fig. 7 shows the polarization curves in the absence and presence of various concentrations of inhibitor. The electrochemical polarization parameters such as corrosion potential (E_{corr}), corrosion current density (i_{corr}), slope of the cathodic branch (β_c), and corresponding percentage inhibition efficiencies ($\eta_{PDP}\%$) were calculated by the Tafel extrapolation method and are listed in Table 5. The values of $\eta_{PDP}\%$ were calculated using the following Eq. 7.

$$\eta_{PDP}(\%) = \frac{i_{corr} - i_{corr(i)}}{i_{corr}} \times 100 \quad (7)$$

Where i_{corr} and $i_{corr(i)}$ are the corrosion current densities for mild steel electrode in the uninhibited and inhibited solutions, respectively.

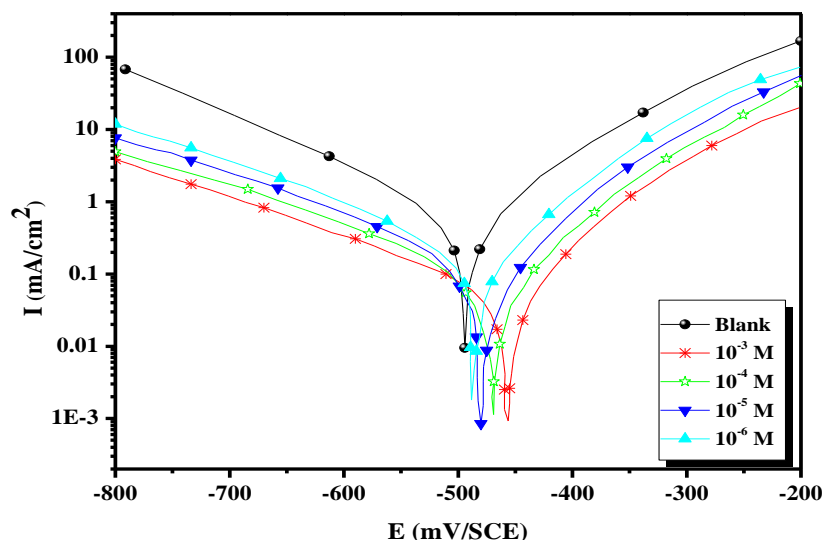


Figure 7: Polarisation curves of carbon steel in 1.0 M HCl for various concentrations of **HBQ8** at 303K.

Clearly, the addition of quinoline derivatives decreased the corrosion current, i_{corr} significantly for all the concentrations studied, correspondingly, η_{PDP} (%) values increase with increasing the inhibitor concentration reaching a maximum value at 10^{-3} M. Moreover, the parallel Tafel curves in Fig. 7 and the almost unchanged values of slope in Table 5 in the absence and presence of inhibitor indicating that the addition of **HBQ8** to the 1.0 M HCl solution did not modify the hydrogen evolution mechanism and the reduction of H^+ ions at the mild steel surface takes place mainly through a charge transfer mechanism [54].

Table 5: Corrosion parameters for corrosion of mild steel with selected concentrations of the inhibitor in 1.0 M HCl by Potentiodynamic polarization method at 303K.

Inhibitor	Concentration (M)	$-E_{corr}$ (mV/SCE)	$-\beta c$ (mV/dec)	i_{corr} ($\mu A/cm^2$)	η_{PDP} (%)	Θ
Blank	1.0	496	162.0	564.0	-	-
HBQ8	10^{-3}	456	180.6	49.1	91.29	0.912
	10^{-4}	469	178.0	84.1	85.02	0.850
	10^{-5}	478	175.0	134.7	76.12	0.761
	10^{-6}	487	161.1	200.3	64.48	0.644

If the E_{corr} values are shifted by > 85 mV in the inhibited system with respect to the uninhibited, the inhibitor could be recognized as cathodic or anodic type, and if the displacement in E_{corr} is < 85 mV, it may be considered as mixed type [55]. In the present case, the addition of the inhibitor caused any significant change in the E_{corr} values suggesting that studied **HBQ8** act as mixed type inhibitor.

3.4. EIS Study

Fig. 8 represents the Nyquist plots for mild steel in the absence and presence of **HBQ8** in 1.0 M HCl at 303 K. It can be observed that all the impedance spectra obtained display one single depressed semi-circle, which indicates that the corrosion process is related to the charge transfer process [16, 18]. The depression in Nyquist semicircles may be due to frequency dispersion, inhomogeneities, and roughness of metal surface and substance transmission actions [11, 12]. The similarity in the shapes of Nyquist plots in the absence and presence of inhibitor reveals that the corrosion mechanism is unaffected by the addition of the **HBQ8**. Furthermore, the diameter of the semicircles in the presence of **HBQ8** is very larger than observed in uninhibited solution and increases with increasing inhibitor concentration, which may be due to the formation of protective film on mild steel surface and consequently reduction in corrosion rate [56].

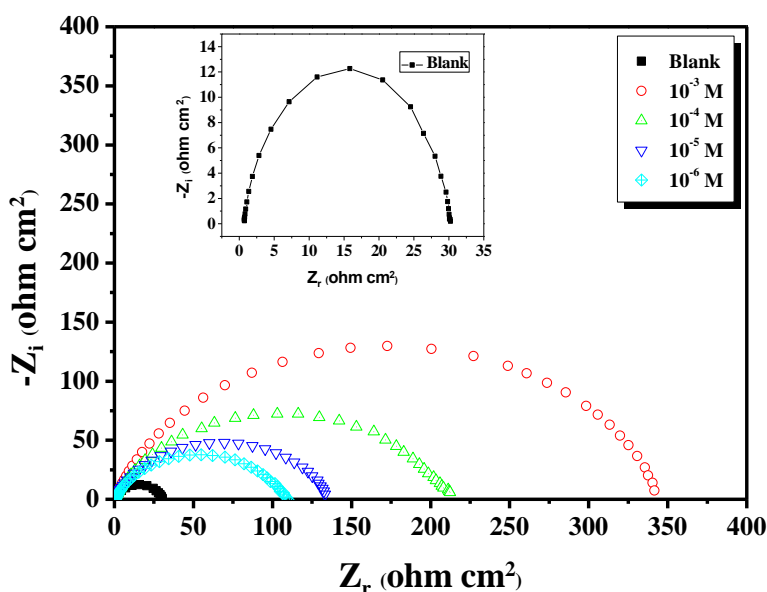


Figure 8: Nyquist curves for mild steel in 1M HCl for selected concentrations of **HBQ8** at 303K.

Accordingly, the *EIS* data are simulated by the proposed equivalent circuit presented in Fig. 9 [57]. It included R_s , the solution resistance, R_{ct} denotes the charge-transfer resistance and CPE is constant phase element. The introduction of CPE into the circuit was necessitated to explain the depression of the capacitance semicircle, which corresponds to surface heterogeneity resulting from surface roughness, impurities, and adsorption of inhibitors. The impedance parameters obtained are reported in Table 6. It has been seen that R_{ct} increased with increase in inhibitor concentrations. Which can be attributed to the formation of an isolating protective film at the metal/solution interface [58]. The CPE impedance is calculated using the Eq. (8)

$$Z_{CPE} = \frac{1}{Q(j\omega)^n} \quad (8)$$

Where Q is the CPE constant (in $\Omega^{-1} \times S n \times cm^{-2}$), ω is the angular frequency (in $rad\ s^{-1}$), $j^2 = -1$ is the imaginary number and n is a CPE exponent which can be used as a gauge for the heterogeneity or roughness of the surface. In addition, the double layer capacitances, C_{dl} , for a circuit including a CPE were calculated by using the following Eq. 9 [59]:

$$C_{dl} = (Q \cdot R_{ct}^{1-n})^{1/n} \quad (9)$$

The inhibition efficiency is calculated from the R_{ct} values using the following Eq. 10:

$$\eta_{EIS} (\%) = \left(\frac{R_{ct} - R_{ct}^0}{R_{ct}} \right) \times 100 \quad (10)$$

Where R_{ct}^0 and R_{ct} are the charge transfer resistances without and with various concentrations of inhibitors respectively.

Table 6: AC-impedance parameters for corrosion of mild steel for selected concentrations of the inhibitor in 1 M HCl at 303K.

Inhibitor	Concentration (M)	R_{ct} ($\Omega \times \text{cm}^2$)	n	$Q \times 10^{-4}$ ($\text{s}^n / \Omega \times \text{cm}^2$)	C_{dl} ($\mu\text{F} / \text{cm}^2$)	η_{EIS} (%)	Θ
Blank	1.0	29.35	0.910	1.7610	91.6	-	-
HBQ8	10^{-3}	346.7	0.909	0.2607	16.2	91.53	0.915
	10^{-4}	209.9	0.910	0.3958	24.6	86.02	0.860
	10^{-5}	134.0	0.922	0.5004	32.8	78.10	0.781
	10^{-6}	105.8	0.898	0.6955	39.8	72.26	0.722

From Table 6, it can be seen that the measured C_{dl} values decreased with increase in inhibitor concentrations. The decrease in C_{dl} values can be attributed to the increase in the electrical double layer at the metal solution interface. This suggests that the inhibitor acts via adsorption at the metal/solution interface [59]. According to Helmholtz model (Eq. 11), the better inhibitive performance of the inhibitors is associated with lower Q value.

$$Q = \frac{\epsilon^0 \epsilon}{d} A \quad (11)$$

Where ϵ is the local dielectric constant, ϵ^0 is the permittivity of the air, d is the thickness of the protective layer and A is the surface area of the electrode. The decrease in Q suggests a fading in local dielectric constant or an increase in the thickness of the electrical double layer, due to the adsorption of quinoline derivative molecules on the mild steel surface by replacement of water molecules by quinoline derivatives molecules [60, 61]. It is worth noting that the experimental results obtained by the EIS measurements are in good agreement with those obtained from weight loss and potentiodynamic polarization.

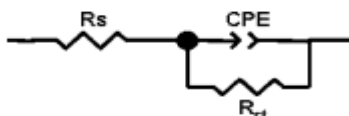


Figure 9: Equivalent electrical circuit corresponding to the corrosion process on the carbon steel in hydrochloric acid.

3.5. Quantum chemical calculation

3.5.1. DFT calculations

It should be stated that DFT methods are widely used in computational chemistry studies because these methods have become very popular in recent times [22, 23]. The input files of quinoline derivative were prepared with Gauss View 5.0.8 [62]. The calculation in the gas phase were made by Gaussian 03W software using DFT/B3LYP method with 6-31G (d, p) basis sets [32, 63]. The structures of **HBQ8** were first optimized using DFT calculations, and then both highest occupied molecular orbital (HOMO) and lowest unoccupied molecular orbital (LUMO) as well as their corresponding energy values (E_{HOMO} and E_{LUMO}) were analyzed.

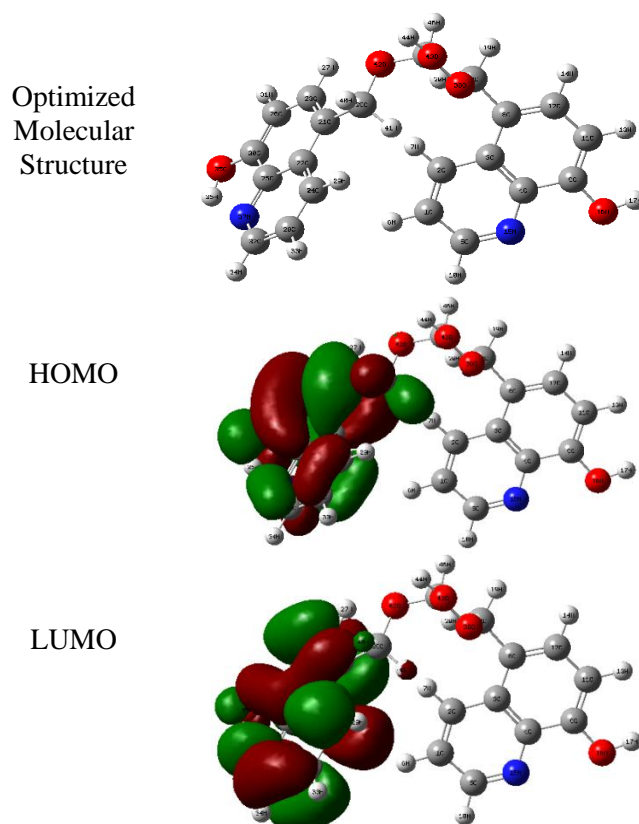


Fig. 10. Quantum chemical results of **HBQ8**, calculated at DFT/B3LYB/6-31G (d, p)

It can be seen from Fig. 10 that the distribution of HOMO and LUMO is localized on the 8-hydroxyquinoline. In the same trend, the reactivity of a molecule is governed by the frontier orbitals. These are the energy of the highest occupied molecular orbital (E_{HOMO}), which indicates the ability of a molecule to donate electrons to an acceptor molecule and the energy of the lowest unoccupied molecular orbital (E_{LUMO}), representing the propensity of a molecule to accept electrons [62]. The difference between the HOMO and the LUMO energies (ΔE) gives an indication of the chemical reactivity of a molecule. The inhibitor with a small ΔE should exhibit a higher interaction with the metal surface⁶⁴. The Table 7 present the parameters obtained by DFT calculation method. For the dipole moment (μ), inhibitor with high dipole moment tend to form strong dipole–dipole interactions with the metal, resulting in strong adsorption on the surface of the metal and therefore leading to greater inhibition efficiency [65, 66]. These conclusions suggests that **HBQ8** is very reactive compound. According to the hard–soft acid base (HSAB) principle, a hard molecule is associated with low basicity and low electron donating ability and a soft molecule is associated with high basicity and high electron donating tendency [67, 68]. This finding suggests that the inhibition efficiency increases with increasing softness and decreases on increasing the hardness of the inhibitor molecules. Absolute electronegativity (χ), global hardness (η) and global softness (σ) are estimated using the equations (Eqs. 12-14) [56, 69].

$$\chi = \frac{I + A}{2} \quad (12)$$

$$\eta = \frac{I - A}{2} \quad (13)$$

$$\sigma = \frac{1}{\eta} \quad (14)$$

The values reported in Table 7 also suggests that **HBQ8** is good reactive compound. The ionization potential (I) and the electron affinity (A) are defined as follows Eqs. 15-16:

$$I = -E_{\text{HOMO}} \quad (15)$$

$$A = -E_{\text{LUMO}} \quad (16)$$

The number of transferred electrons (ΔN) gives information about the number of electrons a molecule can transfer to the acceptor molecule, and it is estimated using the Eq. 17 [23, 70].

$$\Delta N = \frac{\chi_{\text{Fe}} - \chi_{\text{inh}}}{2(\eta_{\text{Fe}} + \eta_{\text{inh}})} \quad (17)$$

where χ_{Fe} and χ_{inh} denote the absolute electronegativity of iron and the inhibitor molecule, respectively, and η_{Fe} and η_{inh} denote the absolute hardness of iron and the inhibitor molecule, respectively. The values of χ_{Fe} and η_{Fe} are taken as 7 eV/mol and 0 eV/mol, respectively. The results, as reported in Table 7, show that the **HBQ8** has the highest tendency to donate electrons and therefore the highest tendency to bind onto the metal surface.

Table 7. The quantum parameters of **HBQ8** calculated using DFT at B3LYB/6-31G (d, p)

Parameter	E_{HOMO} (eV)	E_{LUMO} (eV)	ΔE	η	χ	σ	ΔN	μ (D)
Value	-5.688	-1.557	4.13	2.065	3.623	0.484	0.817	3.075

3.5.2. Molecular dynamic simulation

The molecular dynamics simulations are performed to study the adsorption behavior of **HBQ8** on Fe (1 1 0) surface. Among the three kinds of iron surface (1 1 0, 1 0 0, 1 1 1), Fe (1 1 1) and Fe (1 0 0) surfaces have relatively open structures while Fe (1 1 0) is a density packed surface and has the most stable form [71]. The close contacts between the inhibitor molecules and Fe (1 1 0) surface as well as the best adsorption configuration for the compound are presented in Fig. 11. From this figure, we can conclude that the studied compound can be adsorbed on the Fe surface through the 8-hydroxyquinoline function. A typical plot of energy distribution for inhibitor/Fe (1 1 0) system during energy optimization process consisting of the total energy, average total energy, van der Waals energy, electrostatic energy and intramolecular energy are presented in Fig. 12.

The parameters presented in Table 8 include, the total energy, in kJ/mol, of the substrate–adsorbate configuration. The total energy is defined as the sum of the energies of the adsorbate components, the rigid adsorption energy and the deformation energy, adsorption energy reports the energy released (or required) when the relaxed adsorbate component was adsorbed on the substrate. The adsorption energy is defined as the sum of the rigid adsorption energy and the deformation energy for the adsorbate component. The rigid adsorption energy reports the energy released (or required) when the unrelaxed adsorbate component (before the geometry optimization step) was adsorbed on the substrate. The deformation energy reports the energy released when the adsorbed adsorbate component was relaxed on the substrate surface. Finally, (dEad/dNi) reports the energy of substrate–adsorbate configurations where one of the adsorbate components has been removed [72, 73]. Further, results show that the negative value of adsorption energy for investigated compound support the inhibitive performance of the studied compound and are in accordance with the experimental results.

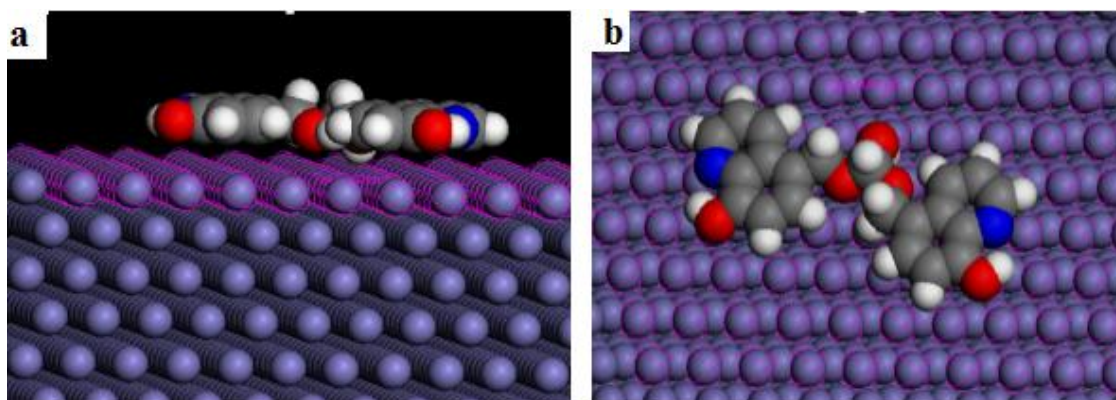


Fig. 11. Side (a) and top (b) views of the most stable low energy configuration for the adsorption of the inhibitor on Fe (1 1 0) surface obtained through the Monte Carlo simulation.

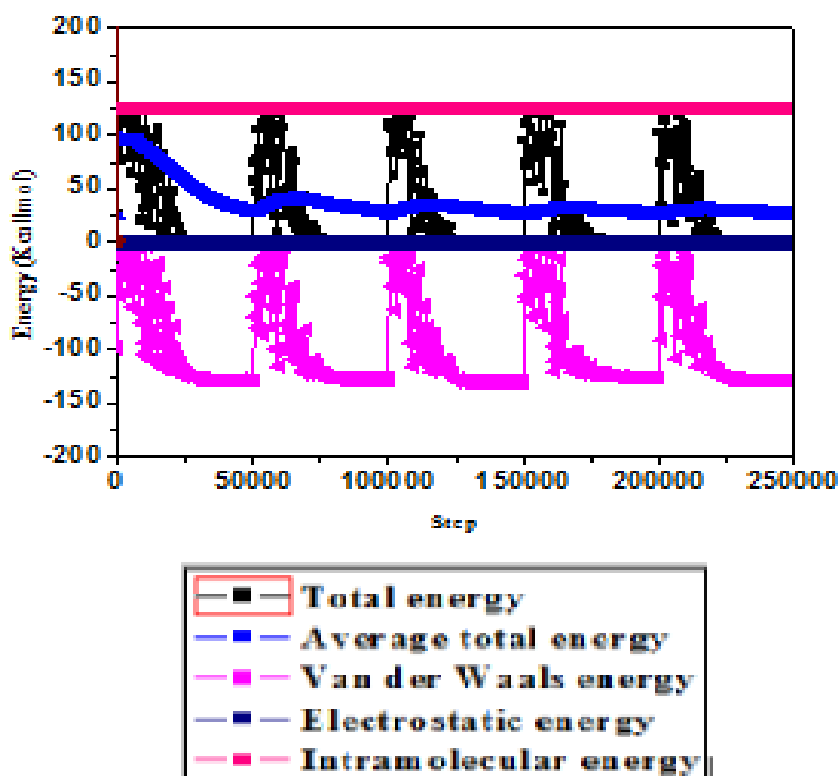


Fig. 12. A typical energy profile for the adsorption progress of **HBQ8** on Fe (110) surface using the Monte Carlo sampling procedure.

Table 8. Outputs and descriptors calculated by the Monte Carlo simulation for the lowest adsorption. Configurations of **HBQ8** /Fe (110) surface (in kcal/mol).

System	Total energy	Adsorption energy	Rigid adsorption energy	Deformation energy	dEad/dNi inhibitor
Fe (1 1 0)/ HBQ8	-29.00	-161.47	-170.20	8.73	-161.47

Conclusion

From the results obtained we can be concluded that **HBQ8** acted as efficient corrosion inhibitor for mild steel in 1 M HCl solution. The charge transfer resistance (R_{ct}) increases and the double layer capacitance (C_{dl}) decreases due to adsorption of the inhibitor molecules on the surface of mild steel. The Polarization studies showed that the studied inhibitor act as mixed inhibitor. The adsorption of the inhibitor on mild steel surface obeys the Langmuir adsorption isotherm and the negative sign of ΔG_{ads}^0 suggests that the inhibitor adsorbed spontaneously on the surface. The Quantum chemical calculations by DFT calculations and Monte Carlo simulation are in good agreement with the experimental results.

References

1. Larouj M., Lgaz H., Serrar H., Zarrok H., Bourazmi H., Zarrouk A., et al. *J Mater Environ Sci* 6 (2015) 3251–3267.
2. Manssouri M., El Ouadi Y., Znini M., Costa J., Bouyanzer A., Desjobert J-M., et al. *J Mater Environ Sci.* 6 (2015) 631–646.
3. Anusuya N., Sounthari P., Saranya J., Parameswari K., Chitra S. *J Mater Environ Sci.* 6 (2015) 1606–1623.
4. Hamdi A., Taouti MB., Benbertal D. *J Mater Environ Sci.* 6(2015) 93–100.
5. khandelwal L., Verma CB., Quraishi MA. *J Mater Environ Sci.* 6 (2015) 810–817.
6. Khelifa A., Hamitouche H., Khadraoui A., Hadj Ziane A. *J Mater Environ Sci.* 6 (2015) 1890–1895.
7. Manimegalai S., Manjula P. *J Mater Environ Sci.* 6 (2015) 1629–37.
8. Kharbach Y., Haoudi A., Skalli MK., Kandri Rodi Y., Aouniti A., Hammouti B., et al. *J Mater Environ Sci.* 6 (2015) 2906–2916.
9. Ghazouani T., Hmamou DB., Meddeb E., Salghi R., Benali O., Bouya H., et al. Antioxidant activity and effect of quince pulp extract on the corrosion of C-steel in 1M HCl. *Res Chem Intermed.* 41 (2015) 1–18.
10. Ouachikh O., Bouyanzer A., Bouklah M., Desjobert J-M., Costa J., Hammouti B., et al. *Surf Rev Lett.* 16 (2009) 49–54.
11. El Makrini B., Lgaz H., Toumiat K., Salghi R., Jodeh S., Hanbali G., et al. *Res J Pharm Biol Chem Sci.* 7 (2016) 2277–2285.
12. El Makrini B., Toumiat K., Lgaz H., Salghi R., Jodeh S., Hanbali G., et al. *Res J Pharm Biol Chem Sci.* 7 (2016) 2286–2294.
13. Toumiat K., El Aoufir Y., Lgaz H., Salghi R., Jodeh S., Zougagh M., et al. *Res J Pharm Biol Chem Sci.* 7 (2016) 1210–1218.
14. El Makrini B., Larouj M., Lgaz H., Salghi R., Salman A., Belkhaouda M., et al. *Pharma Chem.* 8 (2016) 227–237.
15. El Aoufir Y., Lgaz H., Toumiat K., Salghi R., Jodeh S., Zougagh M., et al. *Res J Pharm Biol Chem Sci.* 7 (2016) 1200–1208.
16. Toumiat K., El Aoufir Y., Lgaz H., Salghi R., Jodeh S., Zougagh M., et al. *Res J Pharm Biol Chem Sci.* 7 (2016) 1209–1217.
17. El Aoufir Y., Lgaz H., Toumiat K., Salghi R., Jodeh S., Zougagh M., et al. *Res J Pharm Biol Chem Sci.* 7 (2016) 1219–1227.
18. Krim O., Jodeh S., Messali M., Hammouti B., Elidrissi A., Khaled K., et al. *Port Electrochimica Acta.* 34 (2016) 213–229. Doi: 10.4152/pea.201603213.
19. Afia L., Salghi R., Zarrouk A., Zarrok H., Bazzi EH., Hammouti B., et al. *Trans Indian Inst Met.* 66 (2013) 43–49.
20. Lgaz H., Salghi R., Jodeh S. *Int J Corros Scale Inhib.* 5 (2016) 347–359.
21. Lotfi N., Lgaz H., Belkhaouda M., Larouj M., Salghi R., Jodeh S., et al. *Arab J Chem Environ Res.* 1 (2015) 13–23.
22. Singh RN., Kumar A., Tiwari RK., Rawat P. A. *Spectrochim Acta A Mol Biomol Spectrosc.* 112(2013) 182–190. Doi: 10.1016/j.saa.2013.04.002.

23. Jafari H., Danaee I., Eskandari H., RashvandAvei M. *J Mater Sci Technol.* 30 (2014) 239–252. Doi: 10.1016/j.jmst.2014.01.003.
24. Saadouni M., Larouj M., Salghi R., Lgaz H., Jodeh S., Zougagh M., et al. *Pharm Lett.* 8 (2016) 65–76.
25. Saadouni M., Larouj M., Salghi R., Lgaz H., Jodeh S., Zougagh M., et al. *Pharm Lett.* 8 (2016) 96–107.
26. Fernando Q., Ludekens W., Gnanasoorian K. *Anal Chim Acta.* 14 (1956) 297–299.
27. Lukovits I., Kalman E., Zucchi F. *Corrosion.* 57 (2001) 3–8.
28. Parr RG., Yang W. *J Am Chem Soc.* 106 (1984) 4049–4050.
29. Lee C., Yang W., Parr RG. *Phys Rev B.* 37 (1988) 785–789. Doi: 10.1103/PhysRevB.37.785.
30. Parr RG., Szentpaly L v., Liu S. *J Am Chem Soc.* 121 (1999) 1922–1924.
31. Li X., Deng S., Xie X. *J Taiwan Inst Chem Eng.* 45 (2014) 1865–1875. Doi: 10.1016/j.jtice.2013.10.007.
32. M. J. Frisch, G. W. Trucks, H. B. Schlegel, G. E. Scuseria, M. A. Robb, J. R. Cheeseman, J. A. Montgomery, Jr., T. Vreven, K. N. Kudin, J. C. Burant, J. M. Millam, S. S. Iyengar, J. Tomasi, V. Barone, B. Mennucci, M. Cossi, G. Scalmani, N. Rega, G. A. Petersson, H. Nakatsuji, M. Hada, M. Ehara, K. Toyota, R. Fukuda, J. Hasegawa, M. Ishida, T. Nakajima, Y. Honda, O. Kitao, H. Nakai, M. Klene, X. Li, J. E. Knox, H. P. Hratchian, J. B. Cross, V. Bakken, C. Adamo, J. Jaramillo, R. Gomperts, R. E. Stratmann, O. Yazyev, A. J. Austin, R. Cammi, C. Pomelli, J. W. Ochterski, P. Y. Ayala, K. Morokuma, G. A. Voth, P. Salvador, J. J. Dannenberg, V. G. Zakrzewski, S. Dapprich, A. D. Daniels, M. C. Strain, O. Farkas, D. K. Malick, A. D. Rabuck, K. Raghavachari, J. B. Foresman, J. V. Ortiz, Q. Cui, A. G. Baboul, S. Clifford, J. Cioslowski, B. B. Stefanov, G. Liu, A. Liashenko, P. Piskorz, I. Komaromi, R. L. Martin, D. J. Fox, T. Keith, M. A. Al-Laham, C. Y. Peng, A. Nanayakkara, M. Challacombe, P. M. W. Gill, B. Johnson, W. Chen, M. W. Wong, C. Gonzalez, and J. A. Pople, Gaussian 03, Revision C.02, n.d.
33. Materials Studio. *Revision 6.0*, Accelrys Inc., San Diego, USA; 2013.
34. Kaya S., Tüzün B., Kaya C., Obot IB. *J Taiwan Inst Chem Eng.* 58 (2016) 528–535. Doi: 10.1016/j.jtice.2015.06.009.
35. Khaled KF., El-Maghraby A. *Arab J Chem.* 7 (2014) 319–326. Doi: 10.1016/j.arabjc.2010.11.005.
36. Yüce AO., Kardaş G. *Corros Sci.* 58 (2012) 86–94. Doi: 10.1016/j.corsci.2012.01.013.
37. Keleş H., Keleş M., Dehri İ., Serindağ O. *Colloids Surf Physicochem Eng Asp.* 320 (2008) 138–145. Doi: 10.1016/j.colsurfa.2008.01.040.
38. Hmamou DB., Salghi R., Zarrouk A., Aouad MR., Benali O., Zarrok H., et al. *Ind Eng Chem Res.* 52 (2013) 14315–14327.
39. Mihit M., El Issami S., Bouklah M., Bazzi L., Hammouti B., Ait Addi E., et al. *Appl Surf Sci.* 252 (2006) 2389–2395. Doi: 10.1016/j.apsusc.2005.04.009.
40. Afia L., Salghi R., Bazzi EH., Zarrouk A., Hammouti B., Bouri M., et al. *Res Chem Intermed.* 38 (2012) 1707–1717.
41. Oguzie EE. *Corros Sci.* 50 (2008) 2993–2998. Doi: 10.1016/j.corsci.2008.08.004.
42. Bahrami MJ., Hosseini SMA., Pilvar P. *Corros Sci.* 52 (2010) 2793–2803. Doi: 10.1016/j.corsci.2010.04.024.
43. Lebrini M., Bentiss F., Vezin H., Lagrenée M. *Corros Sci.* 48 (2006) 1279–1291. Doi: 10.1016/j.corsci.2005.05.001.
44. Daoud D., Douadi T., Issaadi S., Chafaa S. *Corros Sci.* 79 (2014) 50–58. Doi: 10.1016/j.corsci.2013.10.025.
45. Lebrini M., Robert F., Vezin H., Roos C. *Corros Sci.* 52 (2010) 3367–3376. Doi: 10.1016/j.corsci.2010.06.009.
46. Moretti G., Guidi F., Fabris F. *Corros Sci.* 76 (2013) 206–218. Doi: 10.1016/j.corsci.2013.06.044.
47. Kharchouf S., Majidi L., Bouklah M., Hammouti B., Bouyanzer A., Aouniti A. *Arab J Chem.* 7 (2014) 680–686. Doi: 10.1016/j.arabjc.2010.12.002.
48. Solmaz R. *Corros Sci.* 81 (2014) 75–84. Doi: 10.1016/j.corsci.2013.12.006.
49. Negm NA., Elkholy YM., Zahran MK., Tawfik SM. *Corros Sci.* 52 (2010) 3523–3536. Doi: 10.1016/j.corsci.2010.07.001.
50. Keleş H., Keleş M., Dehri İ., Serindağ O. *Colloids Surf Physicochem Eng Asp.* 320 (2008) 138–145. Doi: 10.1016/j.colsurfa.2008.01.040.

51. Kharchouf S., Majidi L., Bouklah M., Hammouti B., Bouyanzer A., Aouniti A. *Arab J Chem.* 7 (2014) 680–686. Doi: 10.1016/j.arabjc.2010.12.002.
52. Abiola O., Oforka N. *Mater Chem Phys.* 83 (2004) 315–322. Doi: 10.1016/j.matchemphys.2003.10.001.
53. Wang X., Yang H., Wang F. *Corros Sci.* 53 (2011) 113–121. Doi: 10.1016/j.corsci.2010.09.029.
54. Verma C., Quraishi MA., Singh A. *J Mol Liq.* 212 (2015) 804–812. Doi: 10.1016/j.molliq.2015.10.026.
55. Verma C., Quraishi MA., Singh A. *J Taiwan Inst Chem Eng.* 58 (2016) 127–140. Doi: 10.1016/j.jtice.2015.06.020.
56. Eddy NO., Momoh-Yahaya H., Oguzie EE. *J Adv Res.* 6 (2015) 203–217. Doi: 10.1016/j.jare.2014.01.004.
57. Zhang D., Tang Y., Qi S., Dong D., Cang H., Lu G. *Corros Sci.* 102 (2016) 517–522. Doi: 10.1016/j.corsci.2015.10.002.
58. Khaled KF. *Electrochimica Acta.* 55 (2010) 6523–6532. Doi: 10.1016/j.electacta.2010.06.027.
59. Muthukrishnan P., Prakash P., Jeyaprabha B., Shankar K. *Arab J Chem.* Doi: 10.1016/j.arabjc.2015.09.005.
60. Gupta NK., Verma C., Quraishi MA., Mukherjee AK. *J Mol Liq.* 215 (2016) 47–57. Doi: 10.1016/j.molliq.2015.12.027.
61. Ansari KR., Quraishi MA., Singh A. *Corros Sci.* 79 (2014) 5–15. Doi: 10.1016/j.corsci.2013.10.009.
62. Rodríguez-Valdez LM., Villamizar W., Casales M., González-Rodríguez JG., Martínez-Villafañe A., Martínez L., et al. *Corros Sci.* 48 (2006) 4053–4064. Doi: 10.1016/j.corsci.2006.05.036.
63. Becke AD. *Phys Rev A.* 38 (1988) 3098–3100. Doi: 10.1103/PhysRevA.38.3098.
64. Wazzan NA. *J Ind Eng Chem.* 26 (2015) 291–308. Doi: 10.1016/j.jiec.2014.11.043.
65. Danaee I., Ghasemi O., Rashed GR., Rashvand Avei M., Maddahy MH. *J Mol Struct.* 1035 (2013) 247–259. Doi: 10.1016/j.molstruc.2012.11.013.
66. Ramya K., Mohan R., Anupama KK., Joseph A. *Mater Chem Phys.* 149–150 (2015) 632–47. Doi: 10.1016/j.matchemphys.2014.11.020.
67. Obot IB., Gasem ZM. *Corros Sci.* 83 (2014) 359–366. Doi: 10.1016/j.corsci.2014.03.008.
68. Guo L., Ren X., Zhou Y., Xu S., Gong Y., Zhang S. *Arab J Chem.* Doi: 10.1016/j.arabjc.2015.01.005.
69. Olasunkanmi LO., Kabanda MM., Ebenso EE. *Phys E Low-Dimens Syst Nanostructures.* 76 (2016) 109–126. Doi: 10.1016/j.physe.2015.10.005.
70. Obot IB., Macdonald DD., Gasem ZM. *Corros Sci.* 99 (2015) 1–30. Doi: 10.1016/j.corsci.2015.01.037.
71. Verma C., Ebenso EE., Bahadur I., Obot IB., Quraishi MA. *J Mol Liq.* 212 (2015) 209–218. Doi: 10.1016/j.molliq.2015.09.009.
72. Obot IB., Kaya S., Kaya C., Tüzün B. *Phys E Low-Dimens Syst Nanostructures* (2016). Doi: 10.1016/j.physe.2016.01.024.
73. Khaled KF., El-Maghraby A. *Arab J Chem.* 7 (2014) 319–326. Doi: 10.1016/j.arabjc.2010.11.005.

(2016); <http://www.jmaterenvirosci.com>